Hysteretic Behavior of Angular Dependence of Exchange Bias in FeNi/FeMn Bilayers

T. R. Gao, D. Z. Yang, and S. M. Zhou
The State Key Lab for Advanced Photonic Materials Devices and Department of Physics, Fudan University, Shanghai 200433, China

R. Chantrell
Physics Department, The University of York, York, YO10 5 DD, United Kingdom

P. Asselin
Seagate Research, 1251 Waterfront Place, Pittsburgh, Pennsylvania 15222, USA

J. Du and X. S. Wu
National Laboratory of Solid State Microstructures, Nanjing University, Nanjing 210093, China
(Received 23 December 2006; published 30 July 2007)

For FeNi/FeMn bilayers, the angular dependence of exchange bias shows hysteresis between clockwise and counterclockwise rotations, as a new signature. The hysteresis decreases for thick antiferromagnet layers. Calculations have clearly shown that the orientation of antiferromagnet spins also exhibits hysteresis between clockwise and counterclockwise rotations. This furnishes an interpretation of the macroscopic behavior of the ferromagnetic layer in terms of the thermally driven evolution of the magnetic state of the antiferromagnet layer.

DOI: 10.1103/PhysRevLett.99.057201 PACS numbers: 75.30.Et, 75.30.Gw, 75.60.Jk

Among many key questions of exchange bias (EB) in ferromagnet (FM)–antiferromagnetic (AFM) bilayers, the important role of AFM spins has been studied extensively both theoretically and experimentally [1–6]. The effect of AFM spins on the EB is difficult to clarify due to the zero net magnetization in the AFM layer [7–10]. It is often inferred indirectly through the motion of the FM magnetization with the help of either micromagnetic or classical Heisenberg models [2,3]. Reported results often disagree on the effect of AFM spins on asymmetrical hysteresis loops [2,3,9].

Although the angular dependence of EB (ADEB), specifically the exchange field H_E and the coercivity H_C, has been studied extensively, no special consideration has been made of the sense of rotation of the applied magnetic field H_a [11]. It is assumed *a priori* that the ADEB is identical for clockwise (CW) and counterclockwise (CCW) rotations. For FM/AFM bilayers, however, rotational hysteresis of torque between CW and CCW rotations often exists even for H_a larger than the saturation field of the FM layer because the exchange field acting on AFM spins is smaller than the saturation field of the AFM layer [12,13]. Thus we can surmise a similar affect on the ADEB between CW and CCW rotations. In this Letter, we report on hysteresis of the ADEB between CW and CCW rotations, which decreases with increasing AFM layer thickness t_{AFM}. Calculations show that thermally activated irreversible transitions of the AFM spins are responsible for hysteresis of the ADEB.

A 1 cm $\times$ 5 cm bilayer of $Fe_{20}Ni_{80}$(= FeNi)(3 nm)/$Fe_{50}Mn_{50}$(= FeMn) was deposited on Si(100) at ambient temperature by dc magnetron sputtering from FeNi and FeMn composite targets. The base pressure was 2×10^{-5} Pa and the Ar pressure 0.33 Pa during deposition. Before deposition of the bilayer, a 30 nm thick Cu buffer was prepared to stimulate the EB [14]. Finally, another 30 nm thick Cu layer was used to avoid oxidation. Deposition rates of FeNi, FeMn, and Cu layers were 0.3, 0.1, and 0.2 nm/s, respectively. In order to avoid the run-to-run error, the FeMn layer takes a wedged shape across the distance of 5 cm. Each location along the wedge direction corresponds to a specific t_{AFM}. During deposition, a magnetic field of about 130 Oe was applied parallel to the film plane to induce the EB. Similar fabrication procedure was described elsewhere [15].

X-ray diffraction showed intense and weak peaks at $2\theta = 43.3°$ and 50.6°, corresponding to (111) and (200) preferred orientations of Cu, FeMn, and FeNi layers, respectively. Apparently, constituent layers are polycrystalline with texture. Before magnetic measurements, the specimen was cut into small pieces along the wedge direction prepared at the same time but varying in t_{AFM}. No field cooling was made to avoid morphology degradation at the FM-AFM interface. With a vector vibrating sample magnetometer, m_x and m_y were measured, as components of the magnetic moment parallel and perpendicular to H_a, respectively, where H_a, m_x, and m_y are parallel to the film plane, and m_x corresponds to conventional hysteresis loops. At left and right coercivity, where $m_x = 0$, m_y has maximal values, namely, $m_{y\text{-}L}$ and $m_{y\text{-}R}$. We define $m_{y\text{-av}} = (m_{y\text{-}R} + m_{y\text{-}L})/2$ and the asymmetry factor $\delta = [\mathrm{abs}(m_{y\text{-}R}) - \mathrm{abs}(m_{y\text{-}L})]/[\mathrm{abs}(m_{y\text{-}R}) + \mathrm{abs}(m_{y\text{-}L})]$. During measurements of angular dependence of hysteresis loops, H_a was set to zero during the rotation

of samples. All measurements were performed at room temperature.

Figure 1 shows angular dependence of H_E, H_C, $m_{y\text{-av}}$, and δ for typical FeNi/FeMn bilayer with CW and CCW rotations. ϕ_H is the orientation of H_a, $\phi_H = 0$ defined as the direction at which H_E in CW rotation has its maximum negative value. Apparently, H_C, $m_{y\text{-av}}$, and δ have different angular dependence for CW and CCW rotations. For example, ϕ_H is different for $m_{y\text{-av}} = 0$ between CW and CCW rotations. The angular difference is defined as $\Delta\phi_H$, as shown in Fig. 1(c). It equals 28° for $t_{\text{AFM}} =$ 10 nm. As shown in Fig. 1(a), H_E has almost the same angular dependence for CW and CCW rotations, which will be analyzed below.

As discussed below, the results in Fig. 1 are caused by the hysteresis of ADEB. In order to verify this, another CW rotation was measured *directly* after one cycling of CW and CCW rotations. It is found that the ADEB for the second CW rotation is almost the same as that of the first. Second, $\Delta\phi_H$ is shown to be independent of the increment of ϕ_H between neighboring hysteresis loops. Finally, the ADEB of CW and CCW rotations was measured within different ϕ_H regimes. As shown in Fig. 2(a), the angular dependence of $m_{y\text{-av}}$ is reversible for CW and CCW rotations for small ϕ_H ranges. However, it is irreversible for larger ϕ_H regimes, as shown in Fig. 2(b). Unambiguously, the hysteretic behavior of the ADEB is demonstrated.

Figure 3(a) shows that H_C changes nonmonotonically with t_{AFM}, while H_E changes monotonically, similar to previous results [1]. Figure 3(b) shows that $\Delta\phi_H$ also changes nonmonotonically with t_{AFM}. For bilayers with small t_{AFM}, and also for single FM layers, $\Delta\phi_H = 0$. For $t_{\text{AFM}} > 6$ nm, $\Delta\phi_H$ sharply increases with increasing t_{AFM} to reach a maximum and then decreases.

We have developed a computational model of the hysteretic phenomenon, including thermal activation within the AFM layer. The FM and AFM layers are modeled as a granular microstructure produced using a Voronoi construction (see, for example, [16]). Each layer has the *same* microstructure, which describes realistic systems where columnar growth is continuous across interfaces. The AFM grains are considered exchange decoupled while

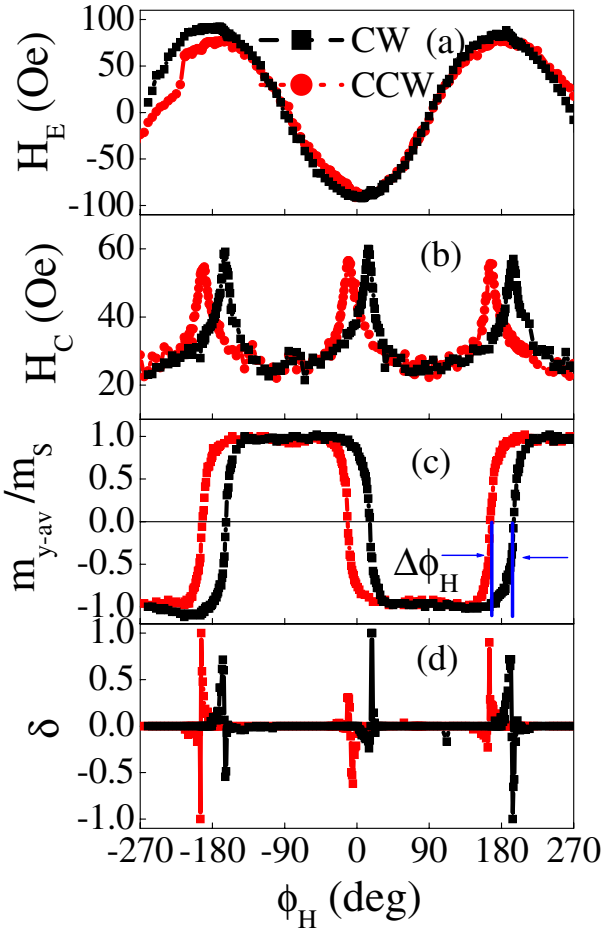

FIG. 1 (color online). Measured angular dependence of H_E (a), H_C (b), normalized $m_{y\text{-av}}/m_s$ (c), and asymmetric factor δ (d) of FeNi(3 nm)/FeMn(10 nm) bilayer for CW and CCW rotations. m_s is the saturation magnetic moment of the sample.

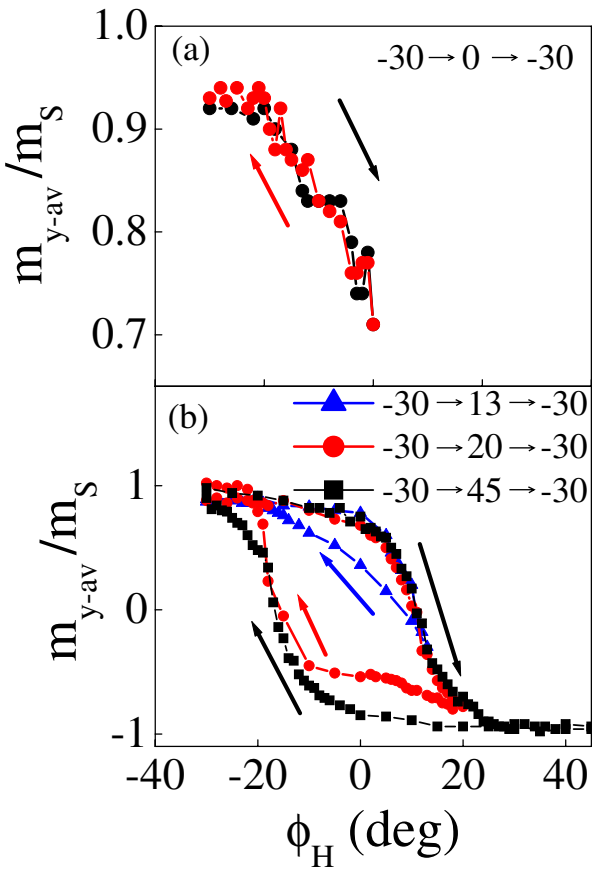

FIG. 2 (color online). Measured angular dependence of $m_{y\text{-av}}/m_s$ for FeNi(3 nm)/FeMn(10 nm) in the ϕ_H region of $-30 \rightarrow 0 \rightarrow -30$ (a), and $-30 \rightarrow 13 \rightarrow -30$, $-30 \rightarrow 20 \rightarrow -30$, and $-30 \rightarrow 40 \rightarrow -30$ (b) in the unit of degrees.

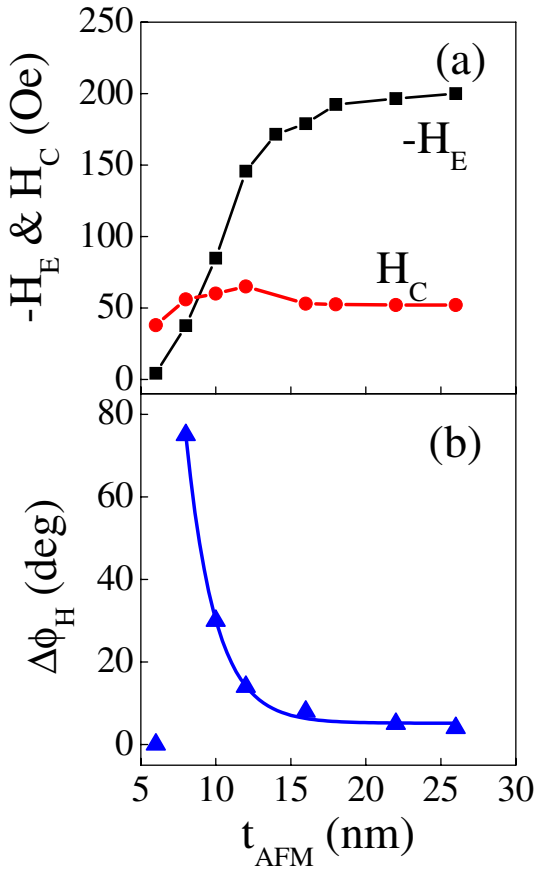

FIG. 3 (color online). Measured dependence of $-H_E$ and H_C at $\phi_H = 0°$ (a) and $\Delta\phi_H$ (b) on t_{AFM} for FeNi(3 nm)/FeMn bilayers. The solid lines serve as a guide to the eye.

neighboring FM-FM and FM-AFM grains are strongly exchange coupled. The AFM layer is treated using a kinetic Monte Carlo algorithm [17]. The *coherent* reversal of AFM spins is governed by thermally activated processes, i.e., the grains are allowed to reverse with a probability p_{sw} given by the Arrhenius-Néel law [18]. In view of the hysteretic behavior of the ADEB, we consider samples with t_{AFM} much smaller than the domain wall thickness and thus neglect planar domain wall in the AFM layer [19]. p_{sw} is determined by the intrinsic energy barrier, i.e., determined by the local anisotropy energy E_{anis}, and the exchange field from the FM layer. $E_{\mathrm{anis}} = a_0 t_{\mathrm{AFM}} K_{\mathrm{AFM}} \sin^2\phi_{\mathrm{AFM}}$, where ϕ_{AFM} is the angle between AFM spins and the easy axis. The anisotropy constant K_{AFM} is single valued, and the lateral area of AFM grains a_0 has a log-normal distribution with a standard deviation $\sigma = 0.3$. The easy axes of the AFM grains are assumed planar randomly orientated. The interlayer exchange energy is [20] $E_{\mathrm{exch}} = -a_0 c_0 J_{\mathrm{int}} \hat{S}_{\mathrm{FM}} \cdot \hat{S}_{\mathrm{AFM}}$, where J_{int} is the interface exchange coupling constant, $\hat{S}_{\mathrm{FM}}$ and $\hat{S}_{\mathrm{AFM}}$ are the unit vectors of the FM and AFM moments at the interface, respectively. The contact fraction c_0 represents the net imbalance of two sublattice magnetizations contacting the FM layer. Determination of stationary states from the total free energy $E_{\mathrm{exch}} + E_{\mathrm{anis}}$ allows calculation of the energy barrier, from which p_{sw} is determined. The FM layer is treated in a standard micromagnetic approach with the cell size being the grain size. The FM grains are coupled with the bulk exchange energy. The magnetic equilibrium state is determined by minimizing the Gibbs free energy, which includes Zeeman, exchange, anisotropy, magnetostatic terms, and interlayer exchange coupling energy. Minimization of the energy is achieved using a conjugate gradient method. The interplay between energy terms allows nonuniform processes to occur.

Figures 4(a)–4(d) show calculations for a system with a median AFM grain size of 5 nm and $\sigma = 0.3$, $t_{\mathrm{AFM}} = 7$ nm, $t_{\mathrm{FM}} = 3$ nm, $K_{\mathrm{AFM}} = 4 \times 10^6$ erg/cm^3, and $K_{\mathrm{FM}} = 5 \times 10^3$ erg/cm^3. For simplicity, it is assumed that $M_{\mathrm{FM}} = M_{\mathrm{AFM}} = 750$ emu/cm^3 and the exchange field between FM-AFM grains is 500 Oe. The present model reproduces major features of the experimental results, except for H_E, for reasons to be discussed shortly.

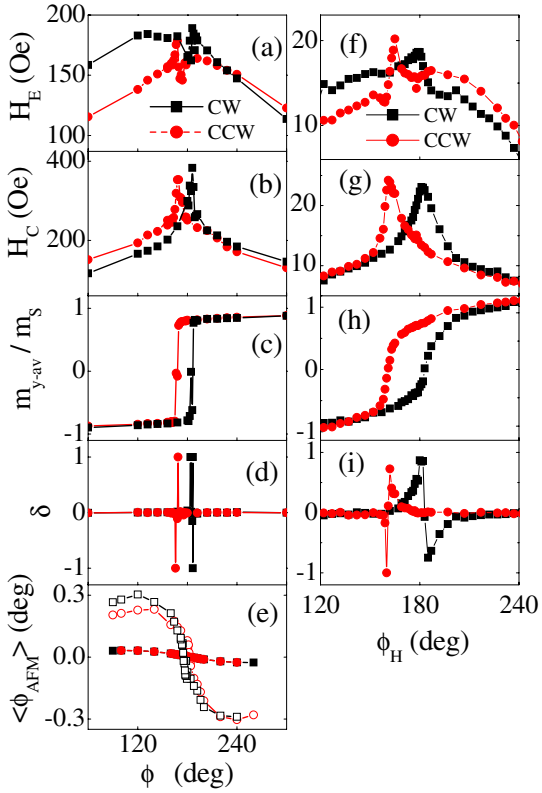

FIG. 4 (color online). Left column: Calculated angular dependence of H_E (a), H_C (b), $m_{\text{y-av}}/m_s$ (c), δ (d) at 300 K, and $\langle\phi_{\mathrm{AFM}}\rangle$ at the state $S1$ throughout CW (squares) and CCW (circles) rotations at 0 K (solid symbols) and 300 K (open symbols) (e) of FM-AFM bilayer. Right column: Measured angular dependence of H_E (f), H_C (g), $m_{\text{y-av}}/m_s$ (h), and δ (i) for typical *uniform bilayer* of FeNi(3 nm)/FeMn(7 nm).

The hysteresis of the ADEB can be explained qualitatively. Consider a hysteresis loop for the FM layer; i.e., $S1(+M_{\mathrm{FM}}) \rightarrow S2(-M_{\mathrm{FM}}) \rightarrow S3(+M_{\mathrm{FM}})$. Calculations show that the average orientation of the AFM spins $\langle \phi_{\mathrm{AFM}} \rangle$ with respect to the direction $\phi_H = 0°$ acquires different values at states $S1$ and $S3$ [21], because AFM spins switch irreversibly during the hysteresis loop of the FM layer. Accordingly, the angular dependence of $\langle \phi_{\mathrm{AFM}} \rangle$ at state $S1$ should show hysteresis between CW and CCW rotations, resulting in an altered magnetic state after CW and CCW rotations. This can be seen from the results at 300 K in Fig. 4(e). On setting the temperature of the AFM layer to 0 K, thereby removing the thermally activated transitions, the rotational hysteresis disappears. Therefore, the rotational hysteresis of the ADEB is suggested to be related to irreversible behavior of AFM spins and induced by thermal activation.

The discrepancy of H_E hysteresis between measured [Fig. 1(a)] and calculated [Fig. 4(a)] results can be explained as follows. The simulations assume a uniform AFM layer, while a wedge-shaped sample is used in experiments. The magnetization reversal process is expected to be accompanied by motion of *single* domain wall for bilayers with wedged AFM layers [15], and by *multidomain form* for uniform bilayers [22]. We have measured the ADEB of an FeNi/FeMn bilayer with uniform layers and found, as shown in Figs. 4(f)–4(i), the angular dependence of H_E to show hysteretic behavior between CW and CCW rotations. Therefore, the disappearance of H_E hysteresis in Fig. 1(a) is caused by the wedged AFM layer and the associated magnetization reversal mechanism. Moreover, the present model can reproduce all features of uniform bilayers.

The features of the measured results in Fig. 3 can be qualitatively reproduced by the theoretical model, as analyzed below. For example, calculations have shown that for $t_{\mathrm{AFM}} = 2.5$ nm, 7 nm, and 10 nm, $\Delta\phi_H$ is 0°, 7°, and 0°, respectively, where the lateral size of AFM grains is 5.0 nm. At small t_{AFM}, all AFM grains are superparamagnetic; i.e., transitions are freely allowed between two stable states. Thus, the H_C enhancement and $\Delta\phi_H$ are negligible. For large t_{AFM}, the AFM layer becomes thermally stable. However, some grains can be switched by the exchange field from the FM layer contributing a ''uniaxial'' anisotropy which enhances H_C and induces $\Delta\phi_H$. For large enough t_{AFM}, the intrinsic energy barrier is increased further and p_{sw} is suppressed thereby decreasing H_C and $\Delta\phi_H$. Meanwhile, as the fraction of stable AFM grains increases, H_E increases monotonically. The behavior of H_E and H_C is well explained by the current model [23].

It is instructive to compare rotational hysteresis of torque with that of ADEB. First, both reveal motion of AFM spins, in different ways [13]. Second, since the rotational hysteresis of torque also exists in single FM layers [24], it is not unique for FM/AFM bilayers. As a new experimental evidence, however, the hysteresis of the ADEB can exist *only* in FM/AFM bilayers because no such phenomenon exists in single FM layers. As a new signature of the EB, the rotational hysteresis of the ADEB can better reflect the nature of the EB and the motion of AFM spins, in comparison with that of torque.

In summary, as a new signature of the EB, rotational hysteresis of the ADEB between CW and CCW rotations was studied for FeNi/FeMn bilayers. For small t_{AFM}, there is no hysteresis of the ADEB. It occurs for large t_{AFM} and increases with increasing t_{AFM} to reach a maximum. Finally, it decreases. Calculations show that the average orientation of the AFM spins exhibits hysteresis during CW and CCW rotations. This arises from thermally activated transitions of the AFM grains. The remarkable agreement between theory and experiment gives strong support to the granular model of EB in polycrystalline bilayers.

This work was supported by the National Science Foundation of China, National Basic Research Program of China, Shanghai Science and Technology Committee.

[1] J. Nogues and I. K. Schuler, J. Magn. Magn. Mater. **192**, 203 (1999); A. E. Berkowitz and K. Takano, J. Magn. Magn. Mater. **200**, 552 (1999).
[2] Z. P. Li *et al.*, Phys. Rev. Lett. **96**, 217205 (2006).
[3] B. Beckmann *et al.*, Phys. Rev. Lett. **91**, 187201 (2003).
[4] H. Ohldag *et al.*, Phys. Rev. Lett. **91**, 017203 (2003).
[5] W. Zhu *et al.*, Phys. Rev. Lett. **86**, 5389 (2001).
[6] A. Hoffmann, Phys. Rev. Lett. **93**, 097203 (2004); M. D. Stiles and R. D. McMichael, Phys. Rev. B **59**, 3722 (1999).
[7] A. Scholl *et al.*, Phys. Rev. Lett. **92**, 247201 (2004).
[8] C. L. Chien *et al.*, Phys. Rev. B **68**, 014418 (2003); F. Y. Yang and C. L. Chien, Phys. Rev. Lett. **85**, 2597 (2000).
[9] J. Camarero *et al.*, Phys. Rev. Lett. **95**, 057204 (2005).
[10] E. Arenholz *et al.*, Appl. Phys. Lett. **88**, 072503 (2006).
[11] T. Ambrose *et al.*, Phys. Rev. B **56**, 83 (1997).
[12] O. de Haas *et al.*, J. Magn. Magn. Mater. **260**, 380 (2003).
[13] M. Tsunoda *et al.*, J. Appl. Phys. **87**, 4375 (2000).
[14] R. Nakatani, Jpn. J. Appl. Phys. **33**, 133 (1994).
[15] S. M. Zhou *et al.*, Phys. Rev. B **58**, R14 717 (1998).
[16] *Handbook of Discrete and Computational Geometry*, edited by J. E. Goodman and J. O'Rourke (CRC, New York, 1997).
[17] R. W. Chantrell *et al.*, Phys. Rev. B **63**, 024410 (2000).
[18] L. Néel, Ann. Geophys. **5**, 99 (1949).
[19] D. Mauri *et al.*, J. Appl. Phys. **62**, 3047 (1987).
[20] E. Fulcomer and S. H. Charap, J. Appl. Phys. **43**, 4190 (1972).
[21] T. Hughes *et al.*, J. Magn. Magn. Mater. **235**, 329 (2001).
[22] Z. Y. Liu and S. Adenwalla, Phys. Rev. B **67**, 184423 (2003).
[23] D. Choo *et al.*, J. Appl. Phys. **101**, 09E521 (2007).
[24] I. S. Jacobs and F. E. Luborsky, J. Appl. Phys. **28**, 467 (1957).